CHAPTER 4

RESULTS AND DISCUSSION

This chapter will be divided into two main sections. The first section is for PZT thin film study. The latter section discusses the sol-gel based composite thick film study. The film characterizations are detailed in both sections including structural, microstructural and electrical characterization. The polarization hysteresis measurement and dielectric constant are reported with electrical characterization.

4.1 PZT Thin Film Study

For PZT thin film study, the effects of annealing condition and the amount of excess Pb on structure, microstructure and electrical properties of PZT thin films were investigated. To study the effect of annealing conditions, films were annealed in the electrical box furnace with the heating rate of 5° C/min in the range of the temperatures between 600-700°C for 30-60 minutes. To study the effect of the amount of excess Pb, 5 and 10 mole% excess Pb were incorporated into stock solution.

4.1.1 Structural Characterization

The structure and orientations of PZT films were examined using X-ray diffractometer (JEOL:JDX-3530) with monochromatic CuK_{α} radiation. Samples were scanned through 2θ between 20° to 60° using step scan with a

sampling interval of 0.02°. For the 52/48 PZT films, the desirable phase which is perovskite has major peaks at 2θ approximately at 21°, 31°, and 38.2°. The second phase so called an intermediate phase or a pyrochlore-like phase has broad major peaks at 2θ about 29.5°, 34.2°, and 49.2°. Since XRD systems utilized Bragg-Brentano (Cullity 1978) diffractometer (the standard 2θ-θ mode), x-rays can penetrate into the film surface and enter the depth of substrate material. Thus, XRD patterns from the PZT films on the substrate showed both weak peaks from the PZT films and strong substrate peaks. To increase the intensity of weak peaks from the PZT films, the 15-layer deposition of films were applied onto the substrates for XRD characterization in this study. A glancing angle method was also used in this study in order to obtain a better resolution of thin film x-ray peaks without interference from the high intensity substrate peaks. Therefore, a small volume of percentages of residual intermediate phase in the PZT films can be detected. The glancing angle was set 5° of angle between incidences and sample surface.

XRD patterns of the Pt-coated silicon substrate were shown in Figure 4.1. Figure 4.1(a) represented an XRD pattern of the unheated substrate consisted of mainly Pt phase as referred to JCPDS file no.04-0802 (Appendix I). This observation indicated that the Pt layer on silicon wafer showed the (111) preferred orientations. In addition, there was a sharp peak of Pt at 2θ of 36°. There was also an indication of a small peak at 2θ ~42° (as sign as *). It was believed to be an intermetallic compound which might form due to interface reactions during heat treatment (Kim et al. 1994). This peak seemed to grow more as shown in Figure 4.1(b) and (c) after further heat treatment. Besides, (200) oriented Pt peak also appeared after a certain heat treatment.

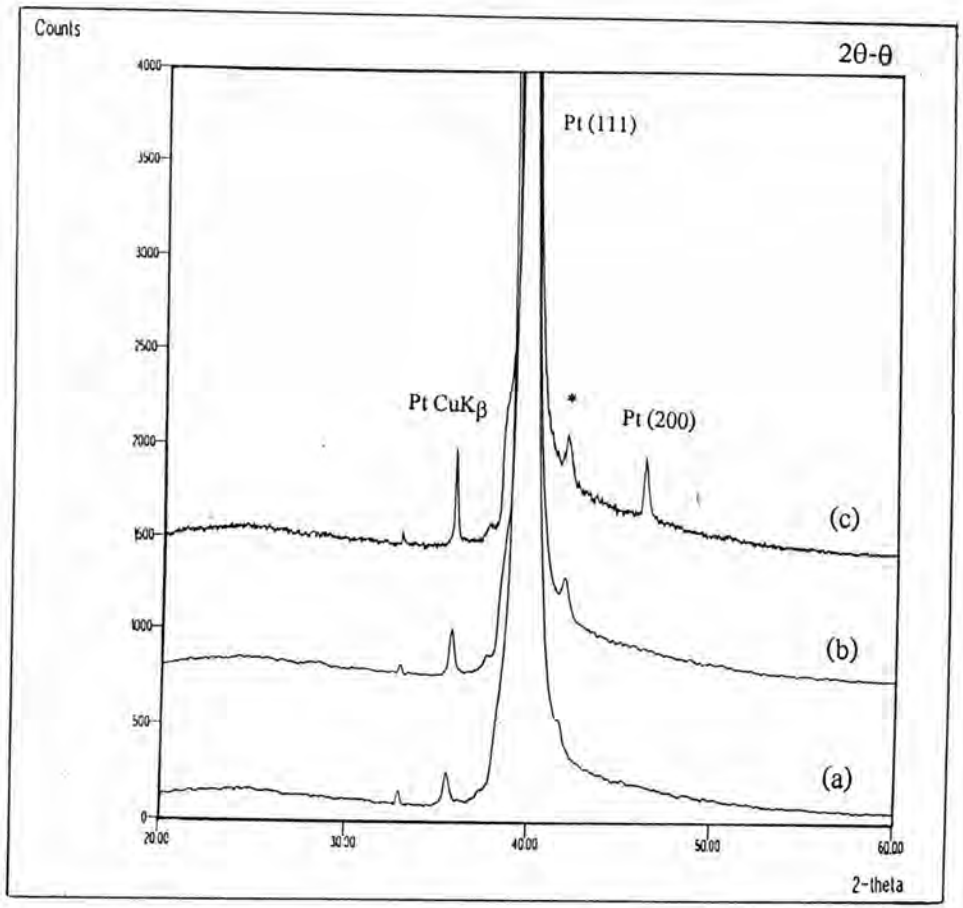

Figure 4.1 XRD patterns of Pt-coated silicon substrates: (a) as-received substrate, (b) heated substrate at 300°C, and (c) heated substrate at 650°C.

It is noted that there is an existence of Pt grown on the substrate after heat treatment (650°C).

XRD patterns of PZT films prepared from solution without adding excess Pb were shown in Figure 4.2. XRD patterns from the as-deposited film, after pyrolysis at 300 °C on the hot plate, only strong peaks from the substrate can be shown in Figure 4.2(a). It can be confirmed that the film was still in amorphous stage. In other word, the crystallization did not occur at 300°C.

Figure 4.2(b), (c), (d) and (e) showed XRD patterns of the annealed films, after such an annealing process at 600 to 700°C for 30 minutes. By applying a glancing angle, it is clear that XRD patterns showed the coexistence of pyrochlore-like phase and perovskite PZT phase. It can be seen that the highest intensity peak of pyrochlore-like phase was in between 28.4 and 30° which covered such a broad area. It is believed that the broad peaks are dued to the small grain size in nanometer size range which is a characteristic of the intermediate phase or second phase which in this case was pyrochlore (Tuttle et al. 1993 and Kwok and Desu 1993).

The amount of the intermediate phase in the vicinity of 2θ 30° seemed to be reduced after annealing at 700°C for 30 minutes as seen in Figure 4.2(e). The perovskite PZT phase in this study showed nearly random orientation, which XRD patterns matched the JCPDS file no. 33-0784 for $Pb(Zr_{0.52}Ti_{0.48})O_3$. The intermediate phase or pyrochlore-like phase, $Pb_2(Zr_{1-x}Ti_x)_2O_6$, matched the JCPDS file no. 26-0142, for $Pb_2Ti_2O_6$. It was assumed that Zr was partially replaced into the position of Ti of $Pb_2Ti_2O_6$. This implied that Pb volatiled during annealing process resulted in the formation of Pb-deficient which was

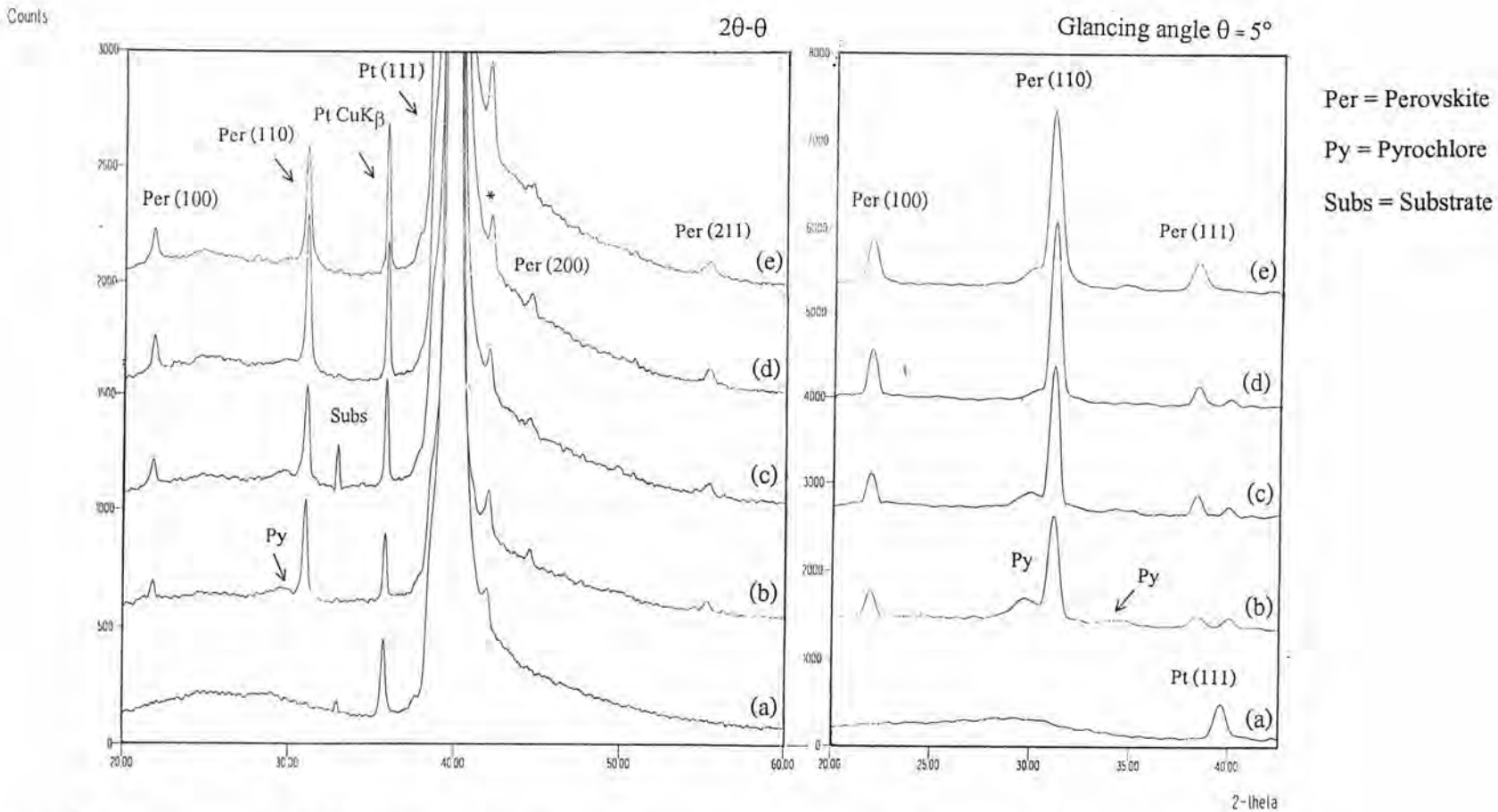

Figure 4.2 XRD patterns of PZT films prepared from solution without adding excess Pb: (a) the as-deposited film (after 300°C pyrolysis), (b) the PZT film annealed at 600°C, (c) at 650°C for 30 minutes, (d) at 650°C for 60 minutes, and (e) at 700°C for 30 minutes.

known as pyrochlore-like or fluorite-type structure and the transformation from intermediate to perovskite phase was not completed. Therefore, an addition of excess Pb in the stock solution was required and would be considered in the followings.

Figure 4.3 showed XRD patterns of PZT films with an addition of 5 molc% of excess Pb annealed at three different conditions. It can be seen that a broad peak of pyrochlore-like phase was observed after 650°C annealing. Eventhough annealing time increased, the pyrochlore-like phase was not able to transform completely to the pure perovskite phase. From the 2θ-θ analysis, XRD patterns of PZT film annealed at 700°C for 30 minutes presented that the broad peak of pyrochlore-like phase disappeared. As further study by glancing angle, indication of an intermediate phase was still observed. However, it could be possible that more adding excess Pb would be required in order to complete the transformation.

Figure 4.4 showed XRD patterns of PZT films with an addition of 10 mole% excess Pb at three different annealing conditions. XRD patterns of PZT film with 10 mole% excess Pb solution showed that the preferred (100) and (111) oriented films were obtained. There was no indication of an intermediate phase after 700°C for 30 minutes heat treatment. This observation confirmed that an addition of excess Pb content and annealing temperature was somehow necessary to complete the transformation.

Therefore, it is reasonable to summarize from these results that the films which were pyrolyzed at 300°C showed amorphous structure. During annealing process, an intermediate or metastable pyrochlore phase first formed

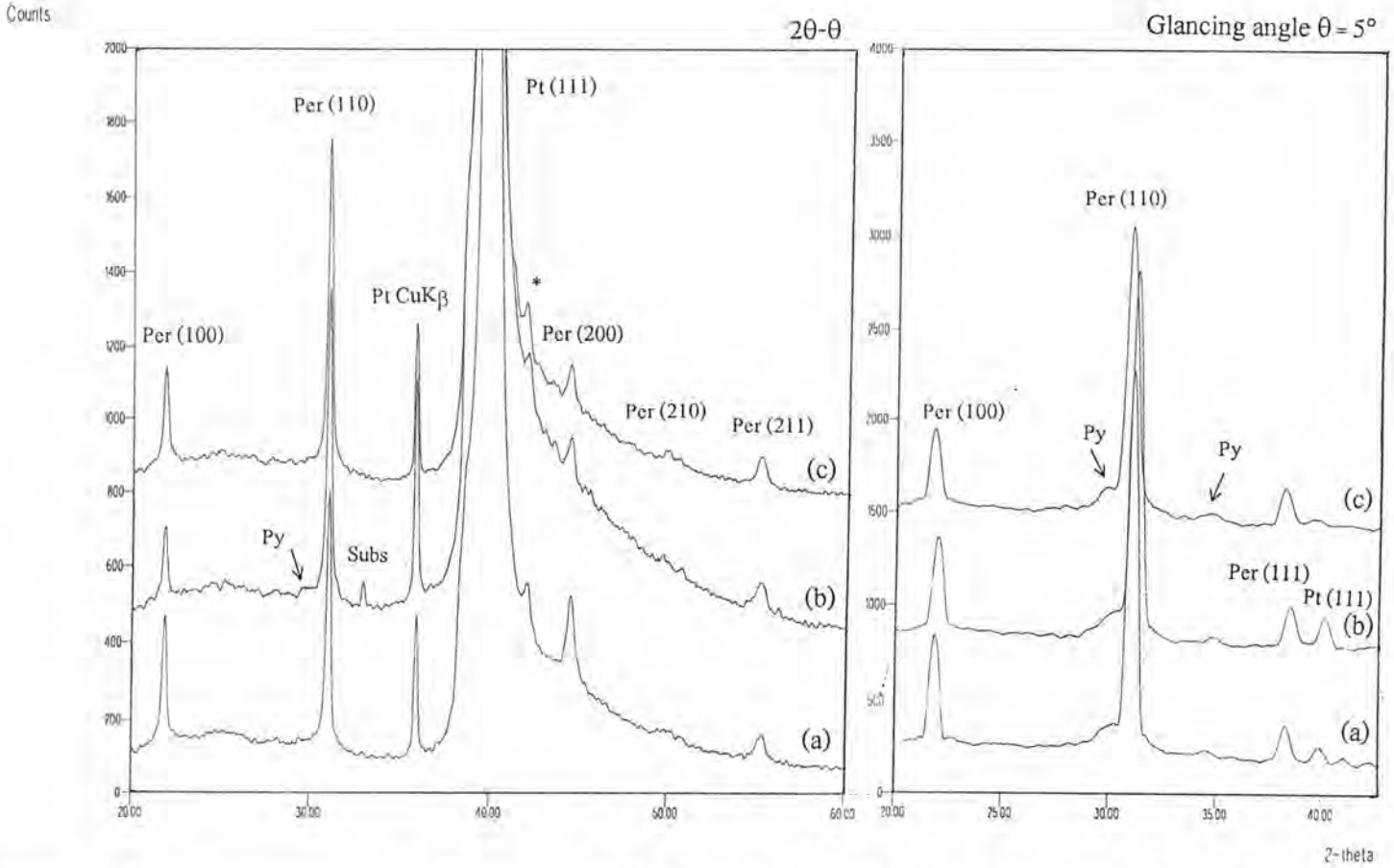

Figure 4.3 XRD patterns of PZT films with an addition of 5 mole% excess Pb made from different annealing conditions: (a) films annealed at 650°C for 30 minutes, (b) 650°C for 60 minutes and (c) 700°C for 30 minutes.

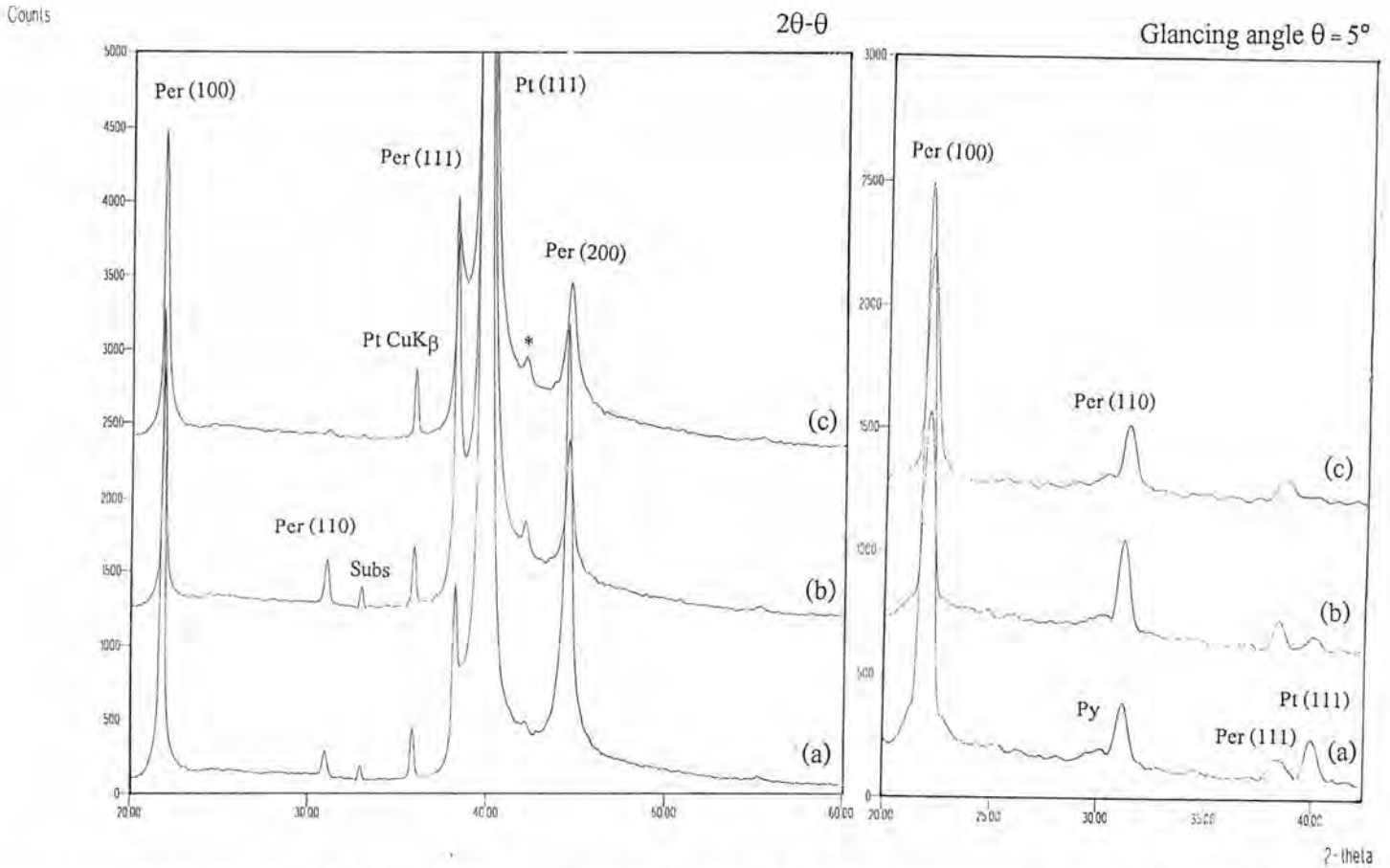

Figure 4.4 XRD patterns of PZT films with an addition of 10 mole% excess Pb made from different annealing conditions: (a) films annealed at 650°C for 30 minutes, (b) 650°C for 60 minutes and (c) 700°C for 30 minutes.

and then transformed to the perovskite phase at higher annealing temperature. However, Pb-deficient pyrochlore phase which could not completely transform to perovskite phase left in films due to Pb-loss during heat treatment. To compensate this loss, therefore, the amount of excess Pb was in corporated into stock solution. This technique enhanced the formation of pure-phase perovskite for a given annealing time and/or temperature which was required for the phase conversion.

4.1.2 Microstructural and Chemical Composition Characterization

Since the primary grain size and cluster of sol-gel PZT thin films which were previously invesigated by Aungkavattana (1996) showed the size range is in nanometer scale. Therefore, a field-emission scanning electron microscope (FESEM) was required to measure film thickness and examine the microstructure of PZT films. Film surfaces were then carbon-coated before taking micrographs using the JEOL (JSM 6301F) microscope with 10-15 KeV accelerating voltage. The magnifications were varied from 3,000X to 25,000X. For Energy dispersive detection system (EDS), 30 KeV accelerating voltage was used to analyze the elements in PZT thin films.

The SEM micrograph of 5-layer-deposited PZT films on Pt-coated Si substrates appeared in Figure 4.5. The film thickness was about 0.3 μm. It can be confirmed that single-layer thickness of an annealed film was approximately 600 Å. It was also showed that the PZT thin film was grown on Pt-coated Si substrate and Pt layer was about 1 μm in thickness.

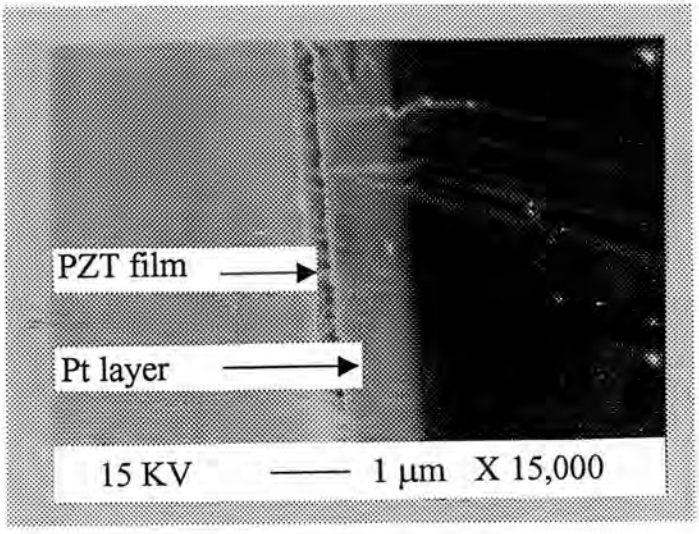

Figure 4.5 SEM micrograph of 5-layer-deposited PZT films on Pt-coated silicon substrate.

Figure 4.6 showed the microstructure of PZT thin films made from the solutions with excess Pb additions ranging from 0 to 10 mol %. These films were annealed at a rate of 5°C/minute at 650°C 30 minutes. It can be observed from the contrast of the micrograph that there were 2 phases of PZT thin films which were made from the solutions with 0 and 5 mole% excess Pb. They consisted of large perovskite rosettes or spherulites embedded in a nanometer grain size pyrochlore matrix.

Because of the higher density, the perovskite phase had a higher secondary electron emission yield and appeared brighter in the SEM micrographs. The microstructures of PZT thin films in this study were similar to these of the previous studies (Hsuch and McCartney 1991, Tuttle et al. 1990, 1992 and 1994). This spherulite crystallite originated from a center, in other words, it nucleated radially from nanocrystalline pyrochlore matrix. Figure 4.6 (a) depicted that films with no excess Pb have a perovskite content less than films prepared from solution with excess Pb. When excess Pb content increased, more spherulites nucleated and coalesced one another at the expense of nanocrystalline pyrochlore matrix.

In 10 mole % Pb excess films, the SEM micrographs presented that the equal size of perovskite phase was much smaller than those of films prepared from solution without and 5 mole% Pb. In addition, the area of nanocrystalline pyrochlore matrix was very small. The pyrochlore phase had existed but it had not been detected by 2θ-θ mode of x-ray diffraction. Study of Tuttle et al. 1992 on transmission electron microscope (TEM) of the PZT films annealed at 550°C reported that the perovskite phase grew from the bottom electrode. The perovskite rosettes were wider at the bottom of the films than at the top of the

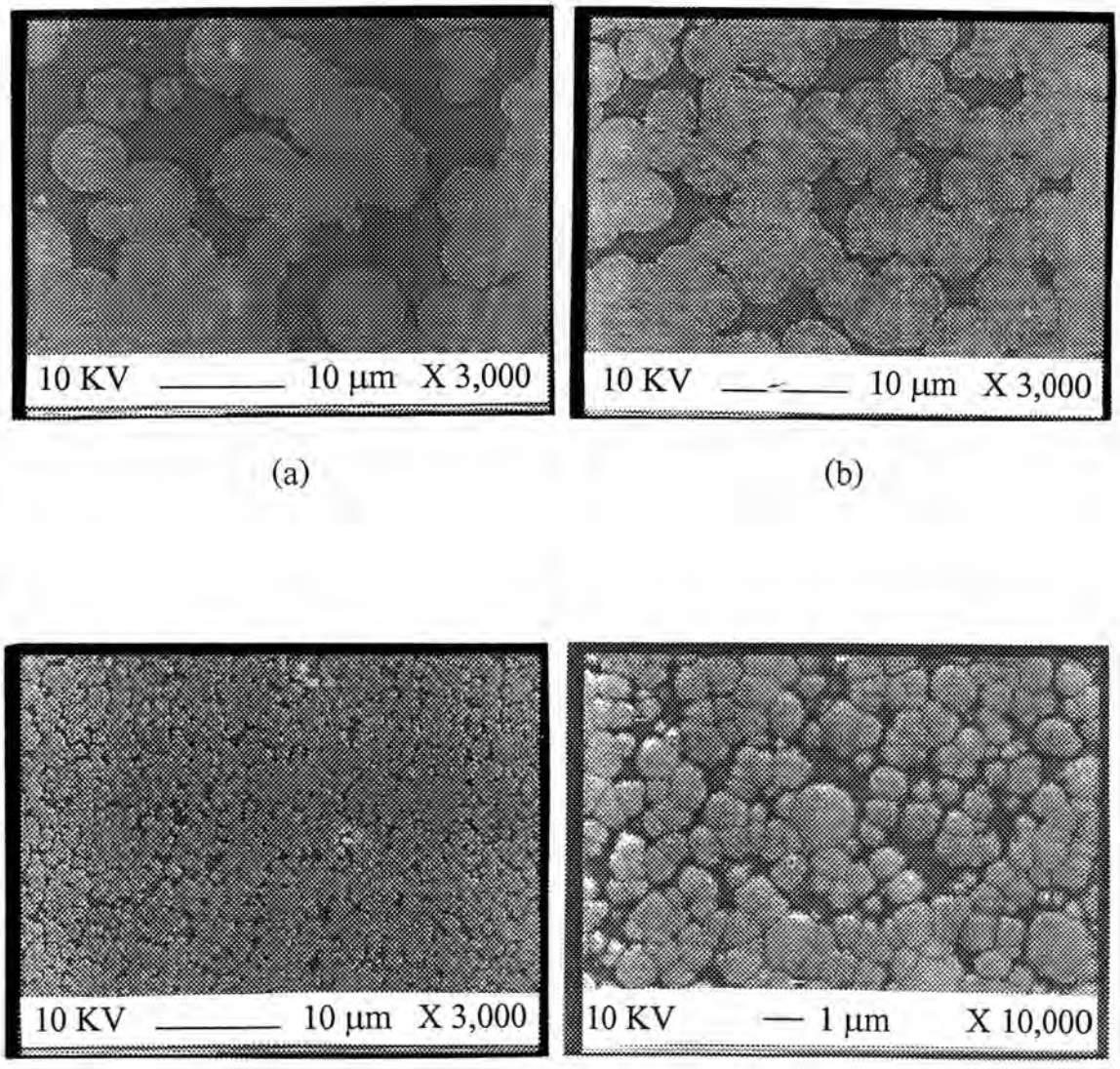

Figure 4.6 Micrographs of PZT thin films annealed at 650°C for 30 minutes: (a) 0 mole%, (b) 5 mole%, (c) and (d) 10 mole% excess Pb.

films. Further examination was confirmed by using glancing angle X-ray diffraction.

The microstructures of films annealed at 650°C for 60 minutes shown in Figure 4.7 were quite similar to films annealed at 650°C for 30 minutes. The SEM micrograph presented that there was no stronger effect of the annealing times to the amount of perovskite phase.

Figure 4.8 showed the microstructure of PZT thin films annealed at 700°C for 30 minutes. The microstruture of films prepared from solution with 0 and 5 mole% Pb excess as shown in Figure 4.8(ā)-(b) were also similar to those of films annealed at 650°C for 30 minutes. In film with 10 mole% Pb excess, when the annealing temperature was increased, more dense PZT films were obtained. The cluster size of sol-gel PZT thin films was approximately 1 μm.

The SEM micrograph presented that an addition of 10 mol% Pb excess was benificial in maintaining the stoichiometry of the PZT films during annealing. Moreover, the intermediate or pyrochlore-like phase can completely transform to perovskite phase after 700°C for 30 minutes heat treatment. However, there was some indication of an intermediate or pyrochlore phase which could not completely transform to perovskite phase in films prepared from the solution with 0 and 5 mole% Pb excess. It may be assumed that %Pb excess was not enough to compensate Pb loss during annealing process.

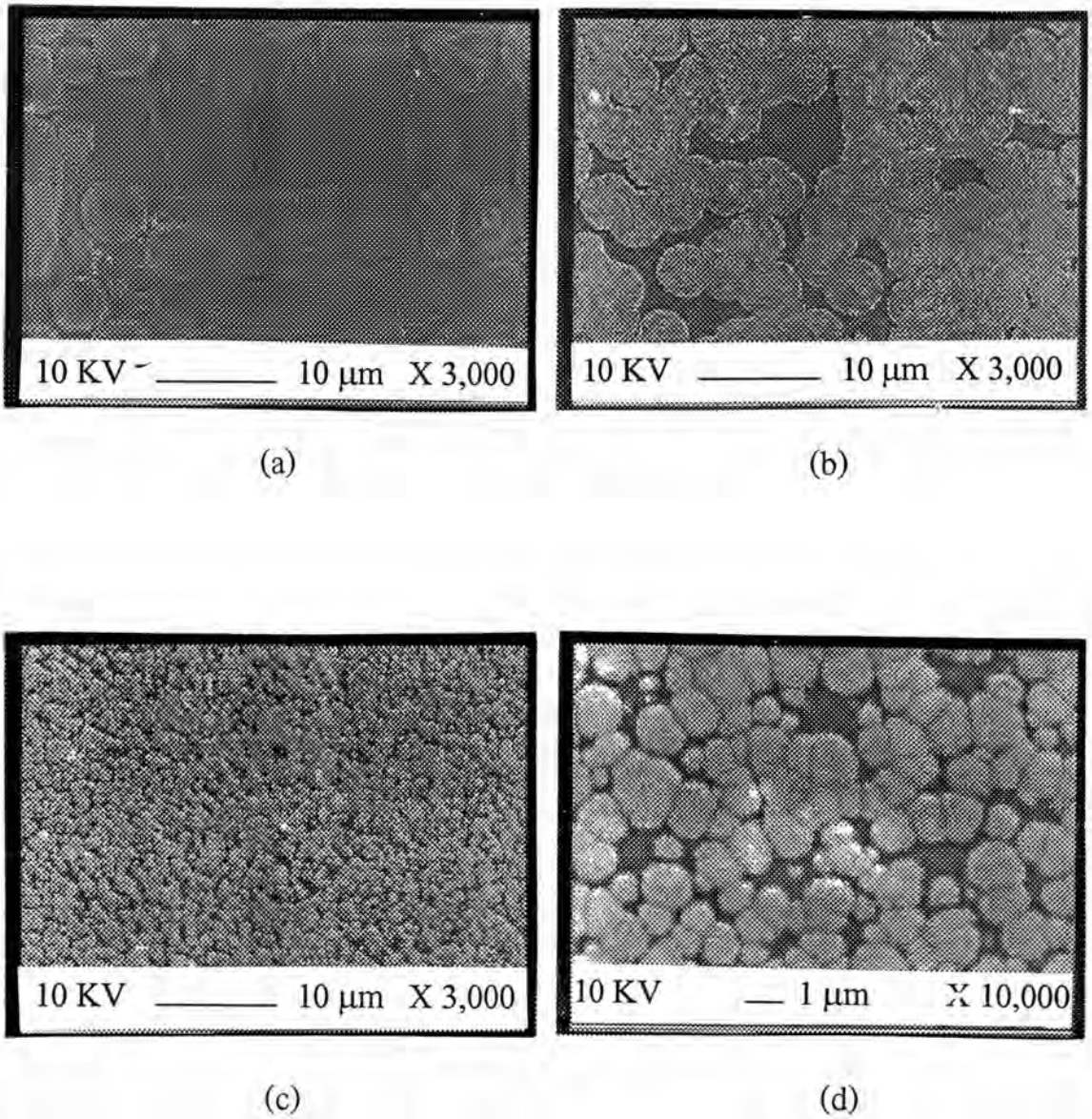

Figure 4.7 Micrographs of PZT thin films annealed at 650°C for 60 minutes: (a) 0 mole%, (b) 5 mole% (c) and (d) 10 mole% excess Pb.

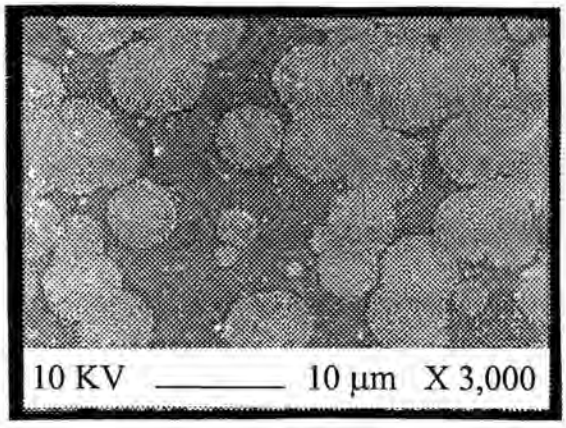

(a)

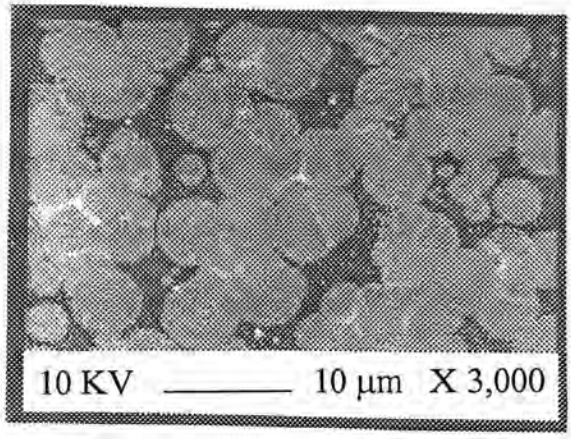

(b)

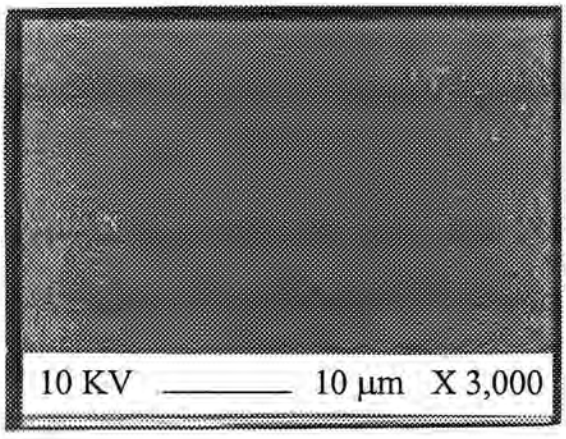

(c)

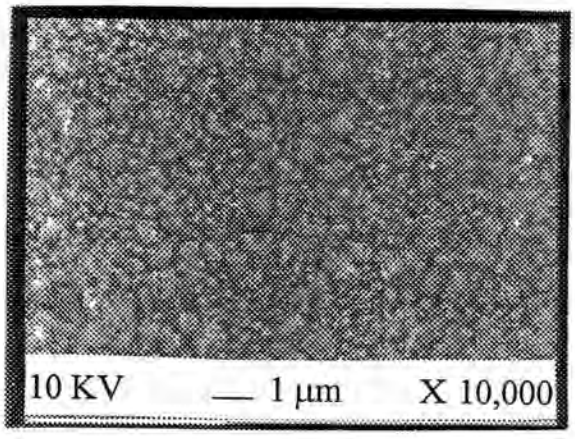

(d)

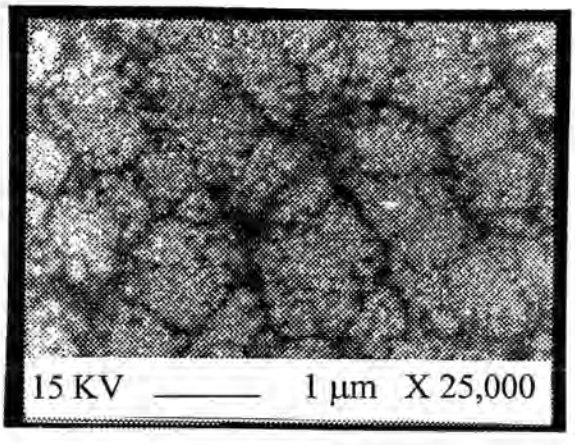

(e)

Figure 4.8 Micrographs of PZT thin films annealed at 700°C for 30 minutes: (a) 0 mole%, (b) 5 mole% (c), (d) and (e) 10 mole% excess Pb.

Figure 4.9 showed SEM micrograph of PZT thin film on platinized silicon substrate annealed at 650°C for 30 minutes. Two distinct features were observed in the microstructure: (a) a region of perovskite phase and (b) a region of intermediate phase. Figure 4.10 showed energy dispersive x-ray spectra from two different regions. EDS X-ray analysis of both regions appeared to have the same Pb, Zr, Ti, O, Pt, and Si element (Appendix II). The energy peaks of Pt and Si elements came from the substrate. However, the exact concentrations of the elements were difficult to obtain because of overlap energy peaks of Pt and Zr.

4.1.3 Electrical Characterization

This section discusses the electrical properties of the PZT thin films. The electrical characterization of the PZT thin films is necessary to determine the film quality. Thus, both the measurements for the polarization hysteresis and dielectric constant were examined in order to measure ferroelectric and dielectric properties of these films. In this study, emphasis is placed on the effect of Pb excess content and the annealing condition. The film thickness in this characterization was approximately 0.3 μm. The hysteresis data of sol-gel PZT thin films prepared in this study were summarized in Table 4.1.

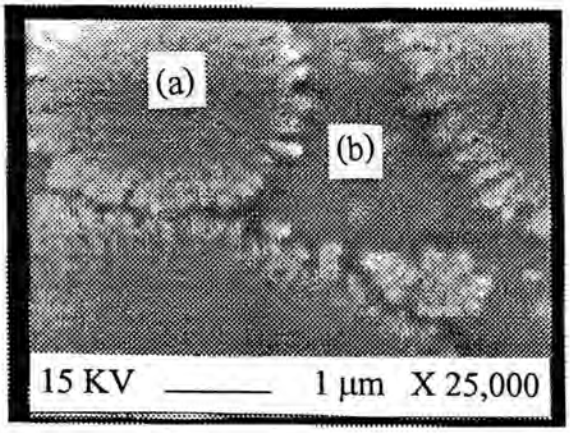

Figure 4.9 Two distinct features in the SEM micrograph: (a) a region of perovskite phase and (b) a region of intermediate phase.

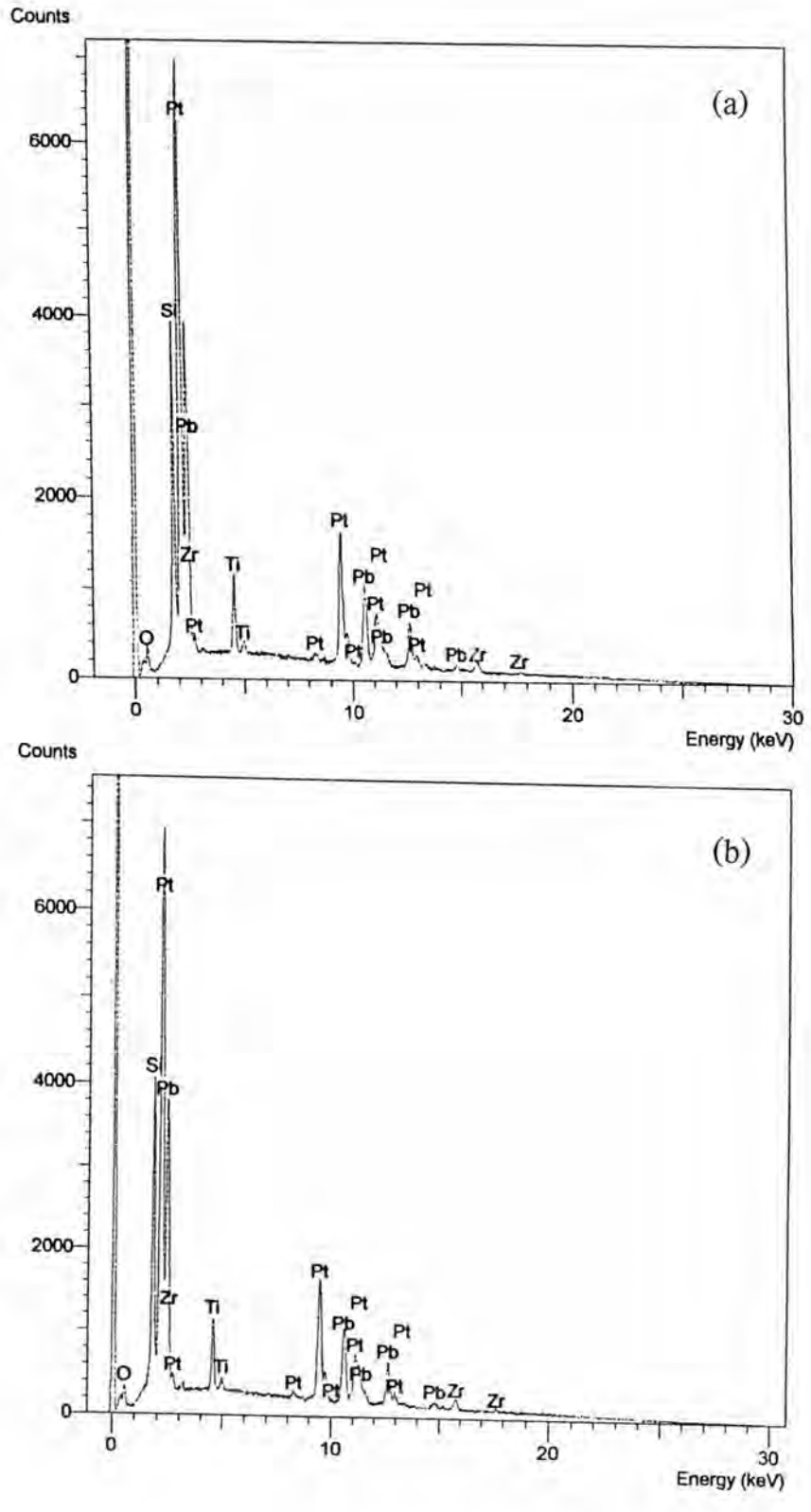

Figure 4.10 Energy dispersive X-ray spectra from (a) the perovskite phase and (b) the second phase.

Table 4.1: The hysteresis data of sol-gel PZT thin films prepared in this study.

mole% excess Pb	annealing condition	Ps ± SD* ($\mu C/cm^2$)	Pr ± SD* ($\mu C/cm^2$)	Ec (kV/cm)
0%	650°C for 30 minutes	13.4 ± 1.4	5.6 ±0.4	39.1 ± 1.0
	650°C for 60 minutes	17.9 ± 1.3	7.1 ± 0.6	32.6 ± 1.2
	700°C for 30 minutes	20.5 ± 0.6	10.4 ± 0.4	41.9 ± 4.3
5%	650°C for 30 minutes	26.6 ± 1.2	10.1± 0.6	38.0 ± 1.3
	650°C for 60 minutes	24.2 ± 1.6	10.4 ± 1.0	32.1 ± 1.0
	700°C for 30 minutes	28.1 ± 1.8	12.3 ± 0.9	35.9 ± 2.6
10%	650°C for 30 minutes	31.5 ± 1.2	12.5 ± 1.1	41.1 ± 3.3
	650°C for 60 minutes	32.1 ± 3.0	12.9 ± 1.0	33.6 ± 3.7
	700°C for 30 minutes	38.1 ± 1.9	19.2 ± 1.1	46.4 ± 2.4

* SD = standard deviation

Figure 4.11 showed the hysteresis loops of sol-gel PZT thin films. The polarization of PZT films with excess Pb additions ranging from 0 to 10 mole% was measured as a function of electric field. The remanent and saturated polarization (P_r and P_s) increased as the percent of excess Pb increased. These results indicated that the amount of excess Pb strongly effected to ferroelectric properties.

When the annealing temperature rised, P_s and P_r of films with 10 mole% Pb excess increased significantly since an addition of Pb excess was enough to compensate Pb loss at higher temperature during heat treatment. Consequently, the intermediate phase can transform almost completely to the desirable perovskite phase.

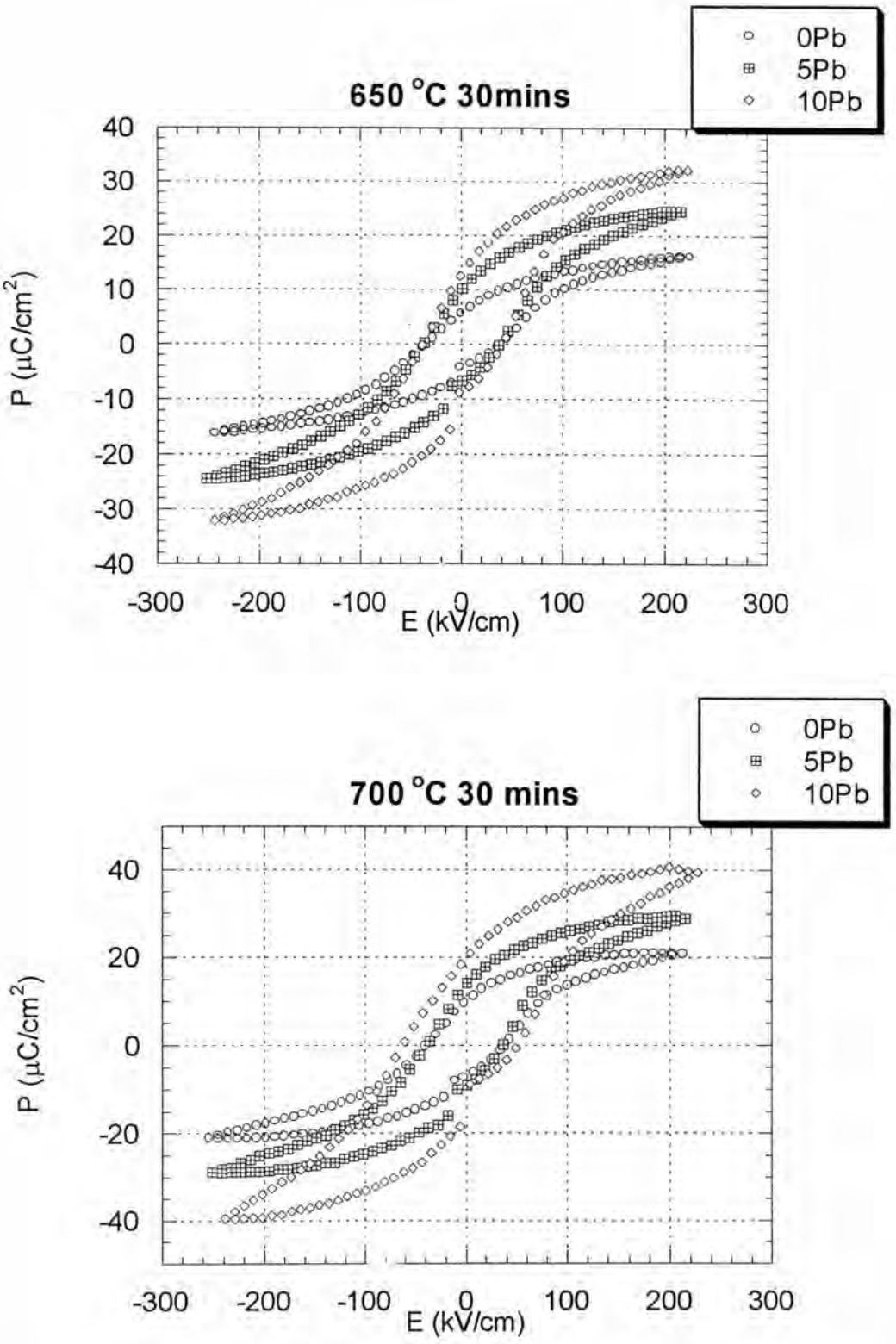

Figure 4.11 The hysteresis loops of sol-gel PZT thin films containing excess Pb ranging from 0 to 10 mole%:(a) films annealed at 650°C and (b) films annealed at 700°C for 30 minutes.

Figure 4.12 showed the hysteresis loops of PZT films with 10 mole% Pb excess at different annealing conditions. Films annealed at 700°C for 30 minutes had significantly better ferroelectric preperties than films annealed at 650°C for 30 and 60 minutes. However, only slight property improvement was obtained as an annealing time increases.

Table 4.2 showed a summary of calculated dielectric constant (K) and dielectric loss (D) found on sol-gel PZT thin films in this study. The calculated dielectric constants of the films agree well with those hysteresis data.

Table 4.2: A summary of calculated dielectric constants and dielectric loss found on sol-gel PZT thin films with a thickness of 0.3 μm.

mole% Pb excess	annealing condition	Capacitance (nF)	Dielectric constant	Dielectric loss
0%	650°C for 30 minutes	1.36 ± 0.13	660 ± 65	0.048 ± 0.005
	650°C for 60 minutes	1.39 ± 0.08	670 ± 40	0.053 ± 0.004
	700°C for 30 minutes	1.49 ± 0.14	720 ± 70	0.065 ± 0.009
5%	650°C for 30 minutes	1.57 ± 0.16	760 ± 75	0.036 ± 0.004
	650°C for 60 minutes	1.56 ± 0.10	760 ± 50	0.059 ± 0.004
	700°C for 30 minutes	1.64 ± 0.16	790 ± 80	0.051 ± 0.004
10%	650°C for 30 minutes	1.76 ± 0.16	850 ± 80	0.049 ± 0.007
	650°C for 60 minutes	1.84 ± 0.12	890 ± 60	0.049 ± 0.008
	700°C for 30 minutes	1.93 ± 0.04	940 ± 20	0.068 ± 0.004

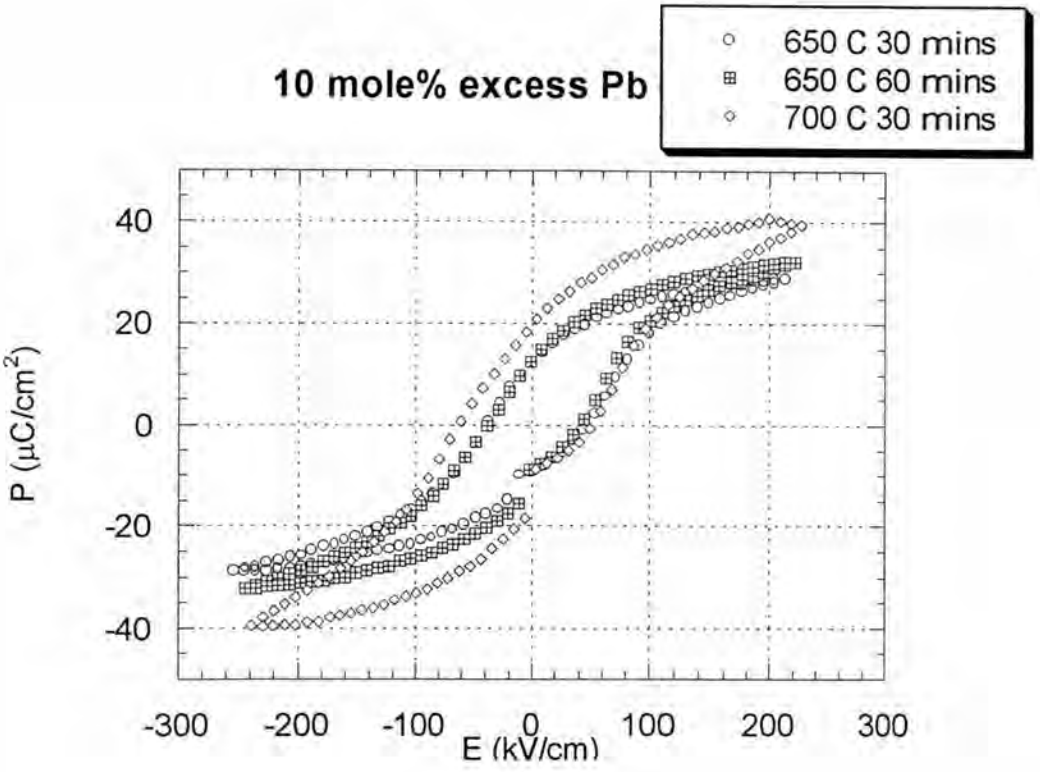

Figure 4.12 The hysteresis loops of sol-gel PZT thin films with 10 mole% excess Pb at different annealing conditions.

In this study, PZT films with containing 10 mole% Pb excess showed good ferroelectric and dielectric properties at the annealing condition of 700°C for 30 minutes. The remanent polarization was 19.2 $\mu C/cm^2$ for an applied voltage of 7 volts. The coercive field was 46.4 kV/cm for films with thickness of 3000 Å. The relatively high dielectric constant was 940 which is comparable to other thin film studies (Hsuch and Mecartney 1991, Toghe et al. 1991, Lakeman and Payne 1992 and Aungkavattana 1996). The good quality films could be due to complete crystallization to a single perovskite phase. These electrical properties corresponded to the uniform and dense microstructure as previously discussed in microstructural study section.

4.2 PZT Thick Film Study

Film thickness in a conventional sol-gel system is generally limited to approximately 500 nm because of the tendency of cracking as thickness approaches 1000 nm. Therefore, sol-gel based composite materials which are made by dispersing PZT powders into a PZT sol-gel solution are used to solve this problem. In PZT thick film study, it will be divided into two parts. The first part is detailed the PZT powder characterization, including the structural characterization and particle size distribution. The latter part is detailed the formulation of paste composition of PZT thick films.

4.2.1 PZT Powder Characterization

Since the thick films are made by dispersing ceramic powders into a sol-gel solution. The resulting composite material or paste composition consisted of a ceramic thin-film matrix with bulk ceramic powders dispersed throughout.

The particle size distribution of PZT powders has to be considered in order to be able to force paste composition through a stencil screen onto the substrate during printing. In addition, structural characterization is also important. It can be confirmed that PZT powders have a desirable crystal structure.

4.2.1.1 Structural Characterization

Figure 4.13 showed XRD patterns of PZT powders fired at 800°C for 4 hours. It can be seen that XRD patterns showed the coexistence of the two perovskite phases (tetragonal and rhombohedral phase) by splitting into triple peaks of $(001)_T$, $(100)_R$, $(100)_T$, $(002)_T$, $(200)_R$, and $(200)_T$. However, it could be observed that there were peaks overlapping between $(102)_R$ and $(102)_T$. This also occurred with $(112)_R$ and $(112)_T$. Consequently, XRD patterns showed double peaks instead of triple peaks (T and R were tetragonal and rhombohedral ferroelectric phase, respectively). The positions of these overlap peaks can be proved by calculating lacttice parameters. The coexistence of tetragonal and rhombohedral phase always occured in $Pb(Zr_xTi_{1-x})O_3$ near the morphotropic phase boundary composition ($0.52 \leq x \leq 0.55$) when prepared by solid-solid reaction among the constituent oxides (Kakegawa et al. 1982).

4.2.1.2 Particle Size Distribution (PSD)

The PSD of PZT powders were demonstrated in Figure 4.14. The results from the analysis were the relative distribution of volume of particles in the range of size classes in which the X- and Y-axes are particle diameter and volume%, respectively. Table 4.3 lists distribution percentiles of PZT powders after milling by high speed attritor at 600 rpm 3 hours. It can be seen that 90%

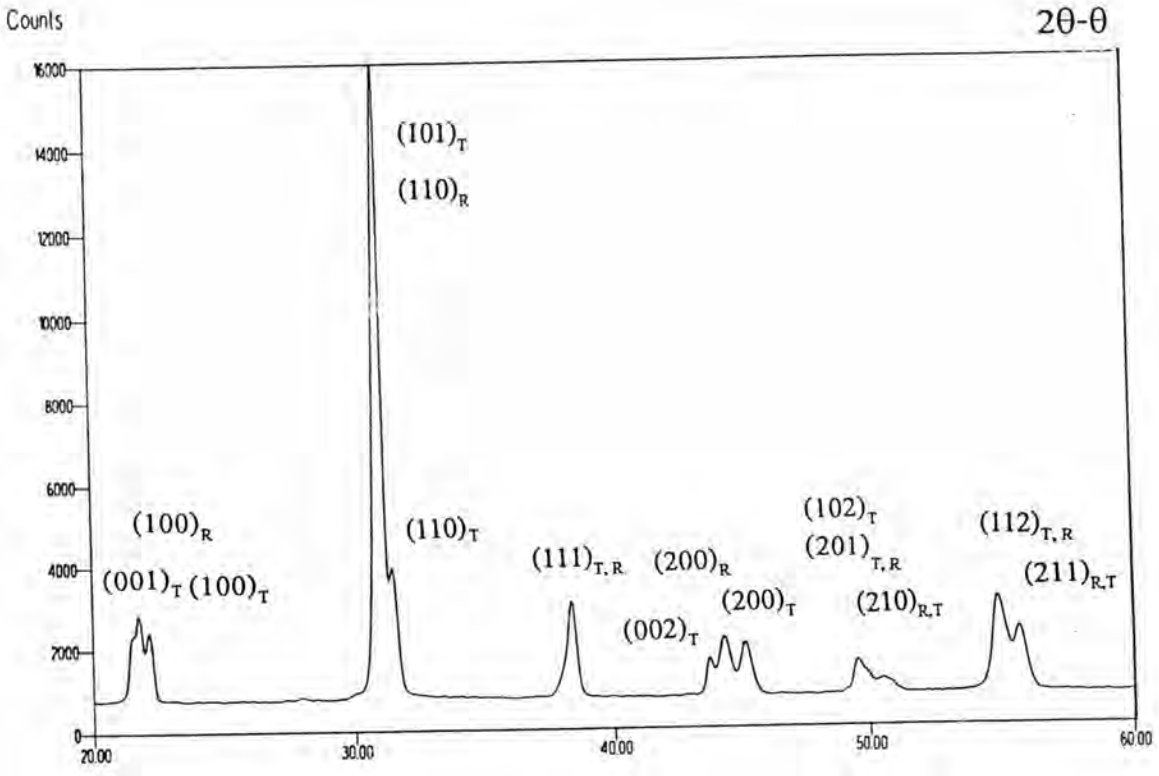

Figure 4.13 XRD pattern of PZT powders sintered at 800°C for 4 hours.

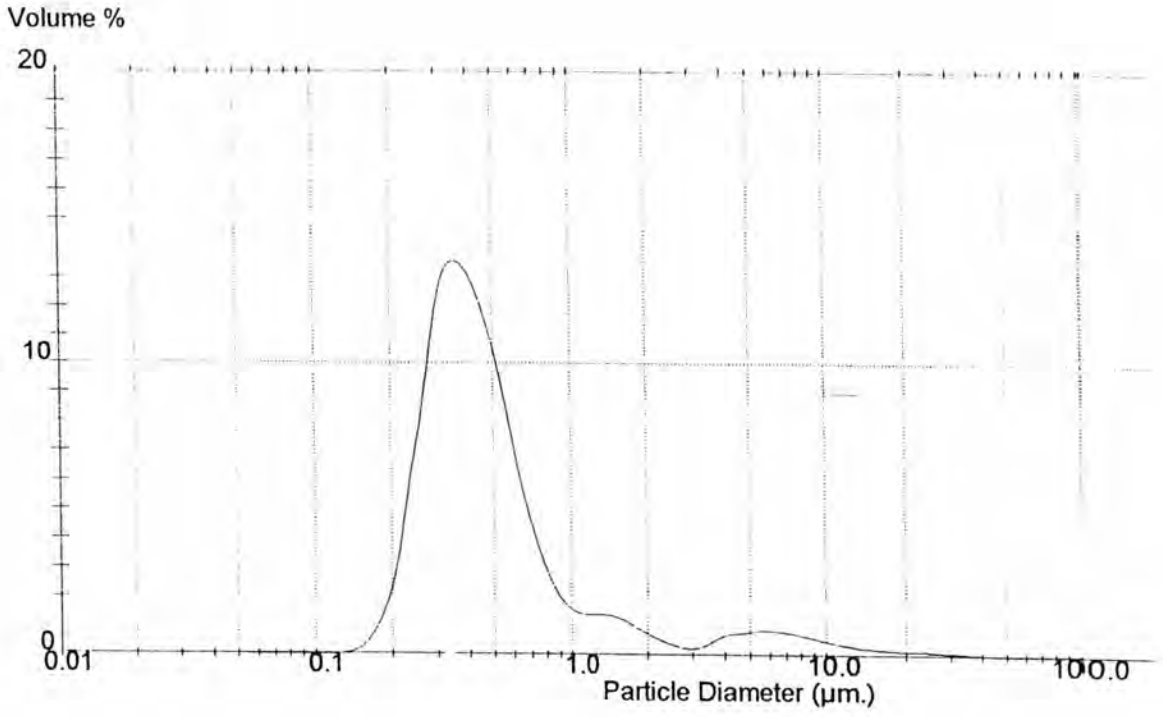

Figure 4.14 Relationship between %volume and particle diameter of PZT powders after high speed milling at 600 rpm for 3 hours by attritor.

by volume of PZT powders are less than 0.9 μm in size. These powders were believed to be suitable for preparation of sol-gel PZT based composite in order to use as ink paste for screen printing.

Table 4.3 Distribution percentiles of PZT powders

Percentile (%)	Size (μm)
10	0.27
20	0.31
50	0.41
80	0.60
90	0.90

4.2.2 Paste Formulation of PZT Thick Films

In this study, paste composition of thick film composed of sol-gel PZT solution and PZT powders. The sol-gel PZT solution at concentration of 0.88M served as an organic vehicle. Ink paste rheology of thick film should exhibit pseudoplastic or thixotropic property which viscosity is an inversion function of shear rate. Therefore, viscosity of paste strongly affecting the print ability was controlled by wt% solid in the paste. In addition, more vol% solid yields high density fired films.

In this study, when %solid loading was more than 75% by weight, the mixture was not able to ball mill effectively to get a homogeneous paste. Therefore, % solid was varied from 70 to 75% by weight. Figure 4.15 showed the relationship between the shear stress and shear rate of pastes at different

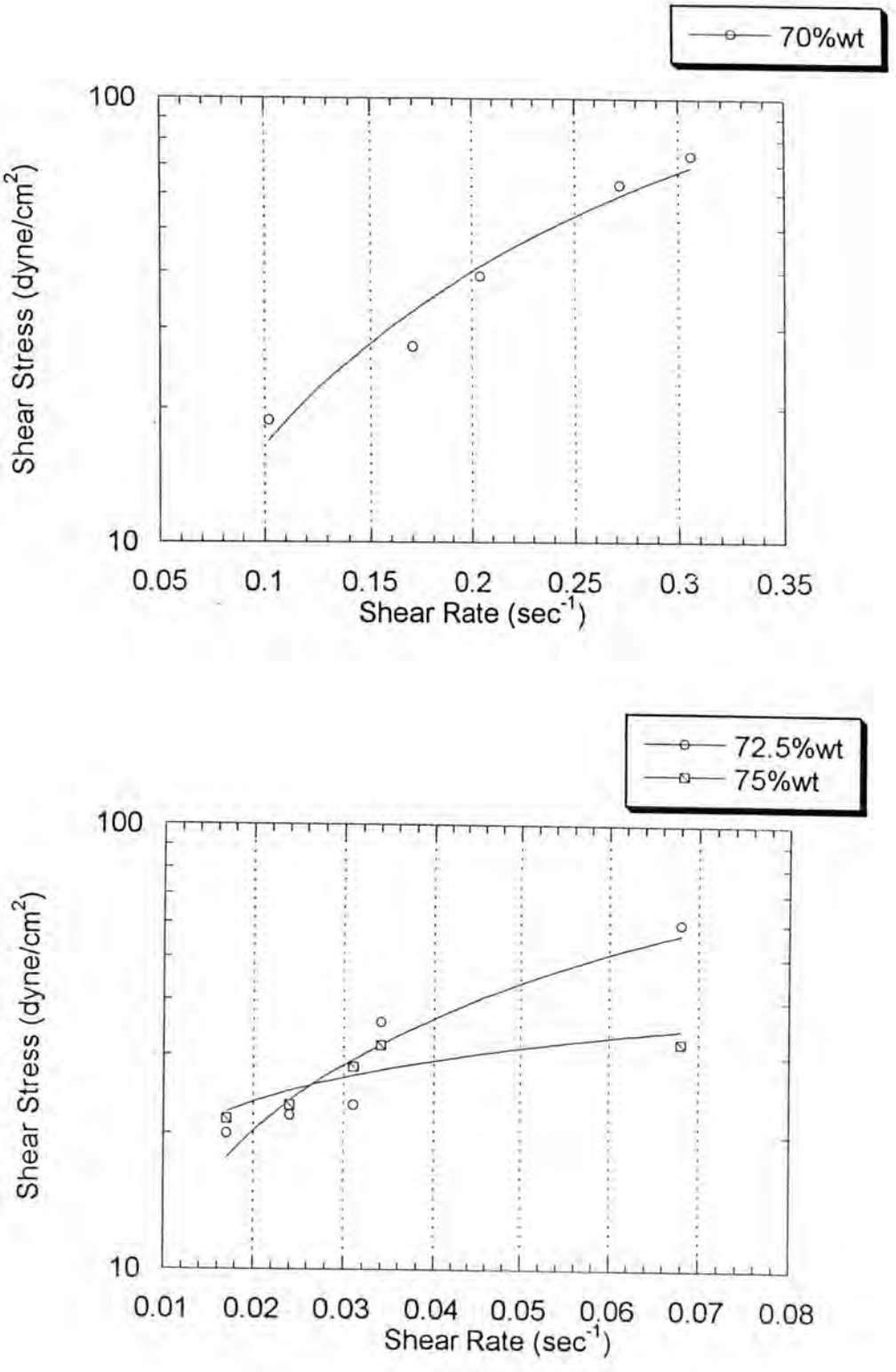

Figure 4.15 The relationship between the shear stress and shear rate of three different pastes.

%solid loading. These results indicated that this paste was pseudoplastic. A summary of print ability of three compositions of paste was shown in Table 4.4.

Table 4.4 A summary of printability of three different pastes.

%solid loading	The range of shear rate (sec^{-1})	The range of viscosity (Pa*sec)	Printability and defects
70	0.102-0.340	18.6-23.5	unable to print, viscosity was too low
72.5	0.017-0.102	58.6-118	be able to print, not smooth pattern
75	0.017-0.102	35.0-172	be able to print, better smoothness on surface